JOURNAL OF GEOPHYSICAL RESEARCH, VOL. 102, NO. D12, PAGES 13,441–13,456, JUNE 27, 1997

Seasonal variation of turbulent energy dissipation rates at high latitudes as determined by in situ measurements of neutral density fluctuations

F.-J. Lübken

Physikalisches Institut der Universität Bonn, Bonn

Abstract. In the last 6 years a series of 22 sounding rockets were launched in order to investigate the dynamic state of the mesosphere and lower thermosphere. Of these flights, 19 were performed at high latitudes, either from the Andøya Rocket Range (17 flights) in northern Norway (69°N) or from Esrange (2 flights) in northern Sweden (68°N). An ionization gauge mounted on board these sounding rockets measured neutral density fluctuations down to very small spatial scales of a few meters. During several flights, small-scale density fluctuations were found in layers of a few kilometers thickness. Subsequent analysis of these fluctuations indicates that they were caused by turbulent motions. The high resolution of these measurements makes it possible to unambiguously deduce turbulent energy dissipation rates ϵ from the spectra of the relative density fluctuations. The ϵ profiles and the corresponding heating rates obtained at high latitudes show a significant and systematic seasonal variation: Whereas in winter the turbulent heating rates are comparatively small (typically 0.1 K/d and 1–2 K/d below and above ~75 km, respectively) in the entire mesosphere and lower thermosphere, much stronger mean values of ~10–20 K/d are observed around the summer mesopause (~90 km). During none of the seven summer flights have we detected any noticeable turbulence in the middle and lower mesosphere. Turbulence is confined to a relatively small height region of 78–97 km during summer but covers the entire mesosphere from 60 to 100 km during winter. From our measurements we arrive at the curious conclusion that turbulent heating in the mesosphere is strongest at the coldest part of the atmosphere, namely, at the polar mesopause in summer. Our observations imply that turbulent heating is an important contribution to the energy budget of the upper mesosphere in summer, whereas it is presumably negligible in the entire mesosphere in winter. Mean turbulent velocities w_{turb} and mean turbulent diffusion coefficients K do not exhibit such a distinct seasonal variation. In the lower and upper mesosphere, typical values for w_{turb} are 0.3 and 1–3 m/s, respectively, and typical values for K are 4 and 100 m^2/s, respectively. The seasonal variation of mean profiles of turbulent parameters as obtained by high-resolution in situ techniques puts a serious constraint on models dealing with the energy budget of the upper atmosphere, in particular the parameterization of subgrid process in terms of mean state quantities, e.g., used in gravity wave breaking scenarios.

1. Introduction

Turbulence is believed to play a major role in upper atmosphere physics and chemistry, since it transports constituents and heat. In addition, it contributes to the thermal budget, since it dissipates kinetic energy into heat, and it is presumably the main mechanism for the deceleration of the mean flow by momentum dissipation. The parameterization of turbulence in models turns out to be difficult for various reasons. For example, phenomena other than turbulence may contribute to the physical process under consideration to an unknown extent, since they cannot be described theoretically, nor can they be measured with techniques available today. A turbulent quantity that has a relatively simple and unambiguous physical interpretation is the turbulent energy dissipation rate ϵ; it can simply be expressed in terms of a temperature increase per unit time. As will be explained later, this quantity is determined unambiguously from our measurements, whereas the derivation of other parameters, such as the turbu-

Paper number 97JD00853.
0148-0227/97/97JD-00853$09.00

lent diffusion coefficient, requires assumptions that cannot be proven with the available data.

To measure turbulence in the upper atmosphere, it would be desirable to measure the velocity fluctuations of the turbulent flow directly. Unfortunately, this is not possible in the middle atmosphere because of experimental limitations. Instead of measuring winds one can also study the fluctuations of a passive tracer caused by turbulent velocity fluctuations. Tracers such as chemoluminescent clouds [*Blamont and DeJager*, 1961; *Rees et al.*, 1972] and chaff clouds [*Wu and Widdel*, 1989; *Lübken et al.*, 1994c] have been released from a rocket, and their spatial and temporal evolution has been investigated in order to measure turbulent diffusion. The problem with these techniques is that nonturbulent effects can disperse the cloud (e.g., from the release process), leading to false quantitative results. Furthermore, the spatial resolution of these techniques is only some tens of meters, a measure that is not sufficient to detect the smallest scales in the turbulence field.

A common technique to obtain information about turbulence is to study its effect on the backscattered signal of a radar. Both the signal strength and the broadening due to turbulent motions have been used [*Gage and Balsley*, 1984; *Hocking*, 1985, 1990]. In deducing quantitative results, uncertainties are introduced, since it is difficult to appropriately correct for nonturbulent effects on the backscattered signal. Furthermore, background parameters needed to deduce quantitative results are normally not measured simultaneously and have to be taken from reference atmospheres. On the other hand, this technique allows for a nearly continuous time coverage of turbulent processes in the upper atmosphere and therefore can be used to qualitatively map the temporal variability of turbulence, e.g., the variation with season. Again, care must be taken, since the "illumination" of the turbulent structures by electrons (required to produce a radar echo) is dependent on season and on ionospheric processes.

More recently, neutral and plasma density fluctuations measured from a rocket have been used as passive tracers for turbulence [*Thrane and Grandal*, 1981; *Blix et al.*, 1990; *Lübken et al.*, 1994c]. The idea behind these measurements is that any vertical excursion of an air parcel due to turbulent motions results in a difference between the number density (neutral or plasma) in the air parcel and that of the environment. This density fluctuation is similar to a passive tracer variation caused by turbulence on a background gradient. The magnitude of the number density fluctuation depends on the strength of turbulence and on the background conditions. The main advantage of these in situ measurements is that the instruments are capable of detecting fluctuations down to spatial scales of a few meters. It turns out that this capability is crucial in deducing quantitative parameters [*Lübken*, 1992]. Another advantage of these techniques is that the background parameters needed to deduce geophysically relevant parameters are measured at the same time and at the same location, either by the same instruments or by accompanying ground-based and/or in situ techniques.

In this study we will consider results from neutral density fluctuations only (and not ions or electrons), mainly because the physical processes causing the plasma fluctuations around the summer mesopause and their relationship to neutral turbulence are not yet understood (see discussion in section 4.2). Recent measurements suggest that ions and electrons are not reliable tracers for neutral gas turbulence under the unique circumstances present around the summer mesopause.

After describing the experimental technique in the next section, we present in section 3 the data available from all our sounding rocket flights. Some of the individual profiles of turbulent parameters have been published in the context of the data presentation for individual campaigns. We will present new data from recent campaigns, and we will derive mean profiles for the summer and for the winter season. A discussion and a comparison of the mean profiles with other measurements and with models are presented in section 4.

2. Method of Observation and Data Analysis

2.1. TOTAL and CONE Sensors

In recent years we have developed two versions of a rocket-borne ionization gauge for in situ measurements of small-scale density fluctuations: The TOTAL and the CONE sensors. The TOTAL sensor (the name indicates that the instrument measures total number densities) is equipped with a closed ion source, where the gas molecules experience several wall collisions before they enter the ionization volume in an accommodation sphere [*Hillert et al.*, 1994]. This ion source geometry limits the time constant for the exchange of gas from the ambient atmosphere to the ion source to approximately 2–8 ms, depending on pressure. To lower this time constant, we have developed the combined neutral and electron sensor (CONE), which is equipped with a system of grids such that the ambient gas molecules enter the ionization region directly (apart from a small percentage being deflected by the grids). The time constant of CONE is below 1 ms [*Lübken*, 1996]. In addition, the CONE instrument is capable of detecting electron density fluctuations with very high time resolution of the order of 1 ms.

Both the TOTAL and the CONE sensors measure neutral density fluctuations in the altitude range from ~115 to ~65 km with a spatial resolution of a few meters and with little instrumental noise, typically less than 0.1% of the total signal. These instruments also measure absolute number densities with the same high-altitude resolution but only in the height range from ~115 to 90 km. The reason for this height limitation

is the unknown effect of atomic oxygen, which reacts with the mechanical components of the sensor and leads to unacceptable uncertainties in total densities above ~115 km. The lower altitude limit is determined by the increasing uncertainty of the so-called "ram correction," which has to be performed in order to convert number densities measured by the sensors to ambient number densities. This correction can be calculated reliably only under free molecular flow conditions, which are fulfilled above ~90 km. Temperatures are derived from the density profile assuming hydrostatic equilibrium (for more technical details on the instruments see *Hillert et al.* [1994] and *Lübken* [1996]). The TOTAL and CONE sensors were mounted on board the Turbulence Bonn Oslo (TURBO) payload, together with other instruments measuring atmospheric quantities relevant to the specific scientific aims of the individual campaigns.

2.2. Background Parameters

Atmospheric mean state background parameters such as temperature and kinematic viscosity are needed in order to deduce turbulent parameters from the measured density fluctuations (see below). In addition, the thermal and dynamical state of the atmosphere can be studied in order to identify possible sources of turbulence. All TURBO sounding rocket flights were accompanied by launchings of meteorological rockets, mainly falling spheres. This technique gives absolute number densities, temperatures, and horizontal winds in the altitude range from ~93 km down to ~30 km with a vertical resolution of a few kilometers [*Jones and Peterson*, 1968; *Schmidlin*, 1991]. The smallest scales detectable by the sphere are typically 7, 3, and 0.8 km at 85, 60, and 40 km, respectively. The uncertainty of the absolute temperature data obtained from the falling sphere is typically 7, 3, and 1.5 K at 90, 80, and 70 km altitude. A comparison between falling sphere measurements and other techniques (e.g., Rayleigh lidar and TOTAL) was performed during the Dynamic Adapted Network for the Atmosphere (DYANA) campaign. It was found that the measurements of the various techniques are reliable and that in general, the error bars given are realistic [*Lübken et al.*, 1994a].

2.3. Data Reduction Procedure

From the neutral density height profile, relative fluctuations $\Delta n/n$ are deduced [*Lübken*, 1992; *Hillert et al.*, 1994], where Δn is the density difference between the air parcel and the environment and n is the mean density. We determine Δn as the difference between the measured densities and a smooth profile, which is obtained from a spline fit in an altitude interval of 1 km (the height interval is increased to 5 km above 85 km to account for the larger kinematic viscosity at high altitudes, which results in larger-scale eddies for a given turbulent intensity).

The magnitude of the density variation for a given vertical excursion Δz is proportional to the square of the Brunt-Väisälä frequency ω_B [*Lübken*, 1992],

$$\frac{\Delta n}{n} \approx \frac{\omega_B^2}{g}\Delta z \tag{1}$$

where g is the acceleration of gravity. This equation presumes that turbulent structures occur in the presence of a stratified background environment. For a given turbulent intensity the magnitude of the fluctuations is expected to be smaller in the summer mesosphere than in the winter mesosphere because of the smaller square of the Brunt-Väisälä frequencies in the summer mesosphere. We will return to this topic in section 4.1. From the relative density fluctuations a power spectrum is calculated, and a theoretical model is fitted to the spectrum (see *Lübken et al.* [1993a] for more details). From the fit we obtain the "break" in the spectrum (called "inner scale" ℓ_o^H), which is unambiguously related to the Kolmogoroff microscale η via

$$\ell_o^H = 9.90 \cdot \eta = 9.90 \cdot \left(\frac{\nu^3}{\epsilon}\right)^{1/4} , \tag{2}$$

where ν is the kinematic viscosity (derived from the background measurements) and ϵ is the turbulent energy dissipation rate, the quantity that we want to determine. The superscript H in equation (2) indicates that this relationship is true only if the theoretical model of Heisenberg is used in fitting the measured spectra. We have also tested a model proposed by *Tatarskii* [1971], which is very similar to the Heisenberg model and basically results in the same ϵ values (see later).

Once ϵ is known, we determine the heating rate

$$\frac{\partial T}{\partial t} = \frac{\epsilon}{c_p} = 0.0864 \cdot \epsilon \quad [\mathrm{K/d}] \tag{3}$$

where $c_p = 1003$ J/(K kg) is the heat capacity of air at constant pressure and ϵ is in milliwatts per kilogram. In addition, we evaluate the mean turbulent velocity w_{turb}, the turbulent diffusion coefficient K, and the outer scale of turbulence L_B, following *Weinstock* [1978, 1981]:

$$w_{turb} = \sqrt{\frac{\epsilon}{0.49 \cdot \omega_B}} \tag{4}$$

$$K = 0.81\frac{\epsilon}{\omega_B^2} \tag{5}$$

$$k_B = 0.9\frac{\omega_B}{w_{turb}} \quad ; \quad L_B = 2\pi/k_B \tag{6}$$

We note that the derivation of these turbulent parameters (i.e., w_{turb} and K) relies on fairly restrictive assumptions concerning the turbulence field. They are therefore much more uncertain than our ϵ values, which are obtained more or less directly from the observed spectra. Despite the questionableness of w_{turb} and K we have determined these parameters, since they are

commonly derived by other techniques (e.g., by radars, with similar uncertainties) and are used for intercomparison.

We will later need an estimate of the amount of fluctuations, σ_{exp}, expected for a given turbulent intensity ϵ and a Brunt-Väisälä frequency ω_B. This quantity is given by the integral of the frequency spectrum, where the integration limit at small frequencies (large spatial scales) is given by the vertical extent of our altitude bin ($\omega_{min} = (2\pi v_R)/L_{max}$; v_R is the rocket velocity). The integration cutoff scale at large frequencies is not important, since the contribution from small scales to the integral is negligible. To facilitate computations, we will therefore apply an inertial subrange (ISR) type spectrum, even at very small scales (smaller than the inner scale), where the actual spectrum deviates from an ISR spectrum due to viscous forces. The inertial subrange part of the Heisenberg spectrum used in our data reduction is given by (see *Lübken et al.* [1993a] for more details)

$$W(\omega) = \frac{6\pi}{5\ v_R} \frac{A\ N}{\epsilon^{1/3}} \left(\frac{\omega}{v_R}\right)^{-5/3} \tag{7}$$

Here, $A = 0.0574$ is a numerical constant, and N (not to be confused with the Brunt-Väisälä frequency ω_B) is given by [*Lübken*, 1992]

$$N = \frac{f_\alpha\ B\ Ri\ \epsilon\ \omega_B^2}{Pr\ g^2} \quad , \tag{8}$$

where Ri is the Richardson number, Pr is the turbulent Prandtl number, $f_\alpha = 2$ is another numerical constant, and B is a factor introduced by *Blix et al.* [1990], which takes into account the degree of isotropy of the turbulent fluctuations and can take values between 3 (isotropic) and 1 (horizontally stratified). The normalization of the spectrum in (7) is such that

$$\sigma^2 = \int_{-\infty}^{\infty} W(\omega)\ d\omega \tag{9}$$

where σ is the variance of the fluctuations. Integrating the spectrum in (7) from ω_{min} to infinity yields the magnitude of fluctuations expected:

$$\sigma_{exp}^2 = 2 \int_{\omega_{min}}^{\infty} W(\omega)\ d\omega \tag{10}$$

(the factor 2 stems from the fact that the spectrum is symmetric about $\omega = 0$). Combining equations (7)–(10) yields

$$\begin{aligned} \sigma_{exp} &= \sqrt{\frac{9}{5}(2\pi)^{1/3}\ A} \sqrt{\frac{f_\alpha\ B\ Ri}{Pr\ g^2}}\ \epsilon^{1/3}\ \omega_B\ L_{max}^{1/3} \\ &= 0.0982\ \epsilon^{1/3}\ \omega_B\ L_{max}^{1/3} \end{aligned} \tag{11}$$

In (11) we have used $B = 3$, $Ri = 0.81$, and $Pr = 1$, mainly to be consistent with other publications using these parameters (for a discussion on the physical background and the variability of the constants B, Ri, and Pr, see *Lübken* [1992]; please note that σ_{exp} depends only in a square root law on these parameters). Equation (11) is not valid under convectively unstable conditions where $Ri < 0$.

We want to complete this section by estimating the upper and lower limits for K and ϵ. Certainly, the turbulent diffusion coefficient K cannot be much smaller than the molecular diffusion coefficient D, because, if so, molecular diffusion would destroy turbulent eddies immediately (the corresponding timescales are proportional to K and D, respectively). We therefore get as a rough estimate

$$K_{min} \approx D \tag{12}$$

Since in the atmosphere $D \approx \nu$ numerically, this also gives a lower limit estimate for ϵ, since from equation (5) we get

$$\epsilon_{min} \approx K_{min} \cdot \omega_B^2 \approx \nu \cdot \omega_B^2 \tag{13}$$

We will later compare profiles of ϵ_{min} with our measurements. This lower limit should not be taken too seriously, since the derivation of ϵ_{min} is based on dimensional arguments and results in an order of magnitude estimate for ϵ_{min} only.

2.4. Rocket Flights

The TURBO sounding rockets were launched within coordinated programs ("campaigns") dedicated to specific scientific problems described elsewhere [*Goldberg et al.*, 1993; *Alpers et al.*, 1993; *Lübken and Blix*, 1994; *Offermann*, 1994; *Lübken*, 1997]. The campaigns are listed in Table 1, and the individual TURBO launches within each campaign are listed in Table 2. The TOTAL

Table 1. Campaigns With Launches of the TURBO Payload

Campaign Label	Campaign Period		Location	Latitude	Number of Flights
DYANA	January–March	1990	Biscarosse	44°N	3
DYANA	January–March	1990	Andøya	69°N	6
NLC	July–August	1991	Kiruna	68°N	2
METAL	September–October	1991	Andøya	69°N	6
SCALE	July–August	1993	Andøya	69°N	2
ECHO	July–August	1994	Andøya	69°N	3

Table 2. List of the TURBO Flights

Flight	Date	Time, UT	Location
	DYANA Campaign in 1990		
DAT13	Jan. 22	1115:00	Andøya
DAT50	Feb. 25	1920:00	Andøya
DAT62	March 6	0241:00	Andøya
DAT73	March 8	2253:00	Andøya
DAT76	March 9	0025:00	Andøya
DAT84	March 11	2042:00	Andøya
DBN 1	Feb. 20	0454:00	Biscarosse
DBN 2	March 6	0518:28	Biscarosse
DBN 3	March 13	0421:00	Biscarosse
	NLC Campaign in 1991		
NBT5	Aug. 1	0140:00	Kiruna
NAT13	Aug. 9	2315:00	Kiruna
	METAL Campaign in 1991		
LT1	Sept. 17	2343:00	Andøya
LT6	Sept. 20	2048:00	Andøya
LI9	Sept. 20	2240:00	Andøya
LT13	Sept. 30	2055:15	Andøya
LT17	Oct. 3	2227:30	Andøya
LT21	Oct. 4	0008:00	Andøya
	SCALE Campaign in 1993		
SCT3	July 28	2223:00	Andøya
SCT6	Aug. 1	0146:00	Andøya
	ECHO Campaign in 1994		
ECT2	July 28	2239:00	Andøya
ECT7	July 31	0050:33	Andøya
ECT12	Aug. 12	0053:00	Andøya

The apogee of the flights is approximately 125 km. The latitudes of the launch sites are Andøya (Norway), 69°N; Biscarosse (France), 44°N; Kiruna (Sweden), 68°N.

sensor was used in the first three campaigns (DYANA, Noctilucent Clouds (NLC), and METAL, in which metal layers were studied), whereas the CONE sensor was used in the Scattering Layer Experiment (SCALE) and ECHO (in which radar echoes were studied) campaigns.

As can be seen from Table 2, a total of 22 flights took place in the last few years, 19 of which were performed at high latitudes (Andøya, 69°N, and Kiruna, 68°N). In Figure 1 we show the distribution of the flights at high latitudes as a function of season. We have grouped the flights into "winter" and "summer" before averaging. In particular, we have combined the four flights performed in early August together with the three July flights (all seven flights representing summer), and we attributed the September and October flights to the winter season. The main reason for this grouping is the thermal structure of the upper atmosphere, which exhibits a rather abrupt transition from summer to winter conditions in late August (the temperature profiles are indeed very similar in June, July, and early August but are very different from the rest of the year [*Lübken and von Zahn*, 1991; *Lübken et al.*, 1996]). In addition, the ϵ profiles obtained during July and early August are very similar in their general behavior but are significantly different from the other flights.

3. Seasonal Variation of Turbulent Parameters

3.1. Neutral Density Fluctuations and Spectra

As an example for a height profile of $\Delta n/n$, we show in Figure 2 the relative density fluctuations ("residuals") observed during SCALE flight SCT6 on August 1, 1993. Residual fluctuations exceeding the noise level of approximately 0.1% are observed in the height range 85 to 94 kilometers. The fluctuations are of the order of 1%, which is the magnitude we expect from equation (1) for air parcel excursions of a few hundred meters and Brunt-Väisälä frequencies of approximately 0.02/s. The residuals in Figure 2 exist down to very small spatial scales, as can be seen more clearly from the spectrum of these fluctuations shown in Figure 3. A Heisenberg type theoretical model is fitted to the observed spectrum shown in Figure 3, and the inner scale ℓ_o^H is obtained from the best fit. As can be seen from Figure 3, the observed spectrum is adequately described by a Heisenberg model with an inner scale ℓ_o^H of 27.3 m. Applying equation (2) and taking into account the measured kinematic viscosity of $\nu = 3.5$ m^2/s, this ℓ_o^H corresponds to an energy dissipation rate of ~740 mW/kg and a corresponding heating rate of ~64 K/d. In Figure 3 we have also plotted a Tatarskii spectrum (dotted line), using the ϵ value from above. This theoretical spectrum is very similar to a Heisenberg spectrum and also nicely fits the observed spectrum (see discussion by *Lübken et al.* [1993a]).

Several examples of spectra similar to the one in Figure 3 have been published in the literature; they demonstrate that the spectra observed in turbulent layers are appropriately fitted by theoretical models such as the Heisenberg or the Tatarskii model [*Lübken*, 1992; *Lübken et al.*, 1993a, 1994b; *Hillert et al.*, 1994; *Lehmacher and Lübken*, 1995]. These spectra result in reliable and unambiguous values for the turbulent energy dissipation rates ϵ. On the other hand, turbulence is not everywhere present in the middle atmosphere, as can be seen from Figure 2. In all TURBO flights we find that turbulence is concentrated in layers of a few kilometers thickness and that the major part of the atmosphere shows very little or no turbulent activity.

3.2. Individual Profiles of Turbulent Energy Dissipation Rates

In Figure 4 the altitude profiles of the turbulent energy dissipation rate ϵ (heating rate on the top ab-

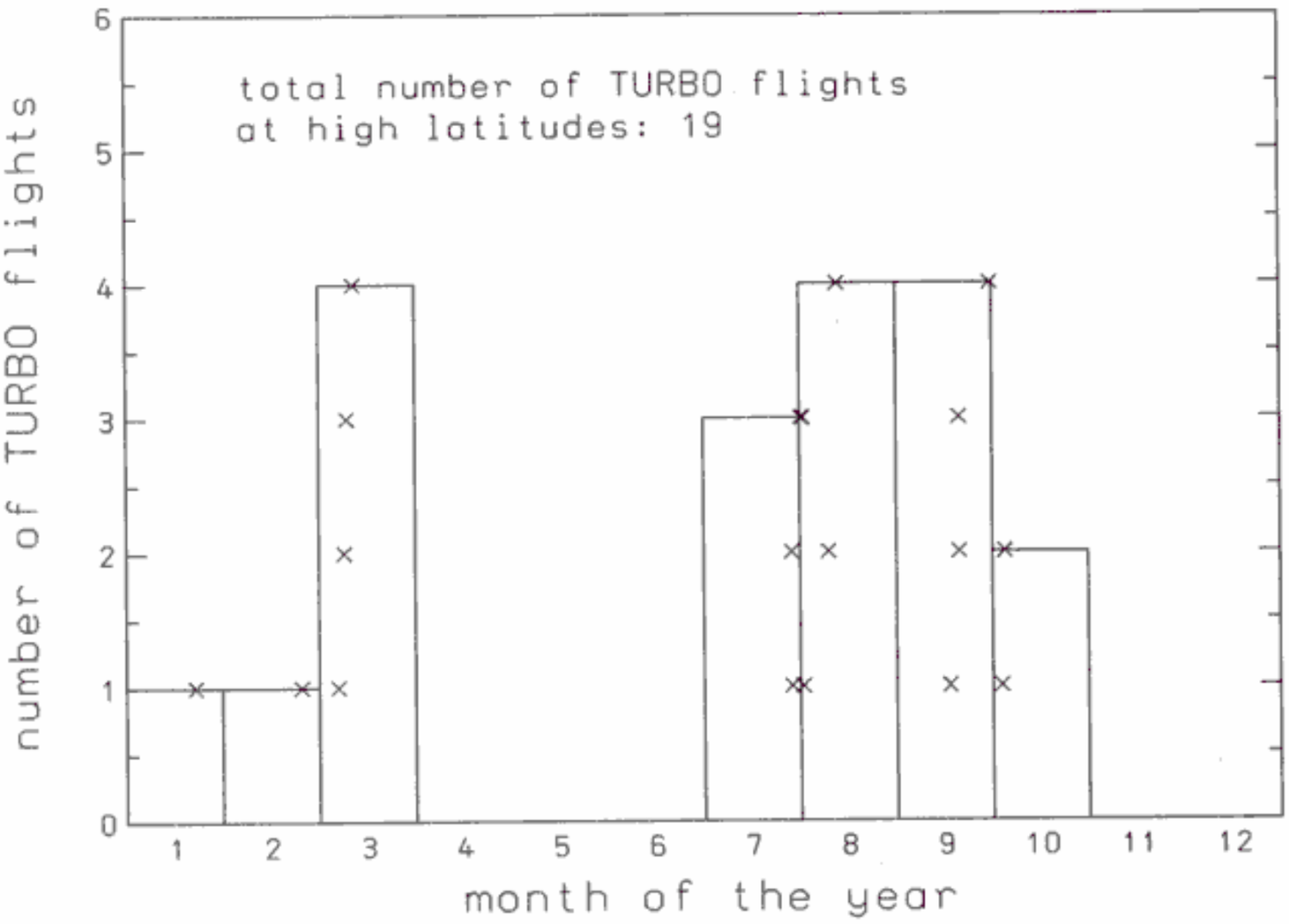

Figure 1. Seasonal distribution of the TURBO flights at high latitudes (Andøya or Kiruna). A total of 19 flights are considered in this plot, which are all the TURBO flights available except the three performed at Biscarosse (44°N). The crosses indicate the times of the various launches within each month.

scissa), the mean turbulent velocity w_{turb}, the estimated turbulent diffusion coefficient K, and the temperature lapse rate dT/dz are shown for the summer flight ECT2 during the ECHO campaign. The general altitude dependence of the turbulent parameters shown in Figure 4 is very similar, a consequence of the close relationship between these parameters through $w_{turb} \propto \sqrt{\epsilon/\omega_B}$ and $K \propto \epsilon/\omega_B^2$ (equations (4) and (5), respectively). Minor differences in the altitude dependence of ϵ, w_{turb}, and K are introduced by their different dependence on the Brunt-Väisälä frequency. In Figure 4 we also show the rough estimate for the minimum theoretical value for ϵ, calculated from equation (13) (for reasons of comparison we have used CIRA (1986) temperatures, not the falling sphere temperatures, to determine ϵ_{min}, since the theoretical uncertainty of ϵ_{min} is much larger than the variability caused by different temperature profiles). The example shown in Figure 4 is typical for a summer profile with rather larger energy dissipation rates of 123 mW/kg around 90 km (corresponding heating rates of ~10 K/d). No turbulent activity is detected in the lower mesosphere.

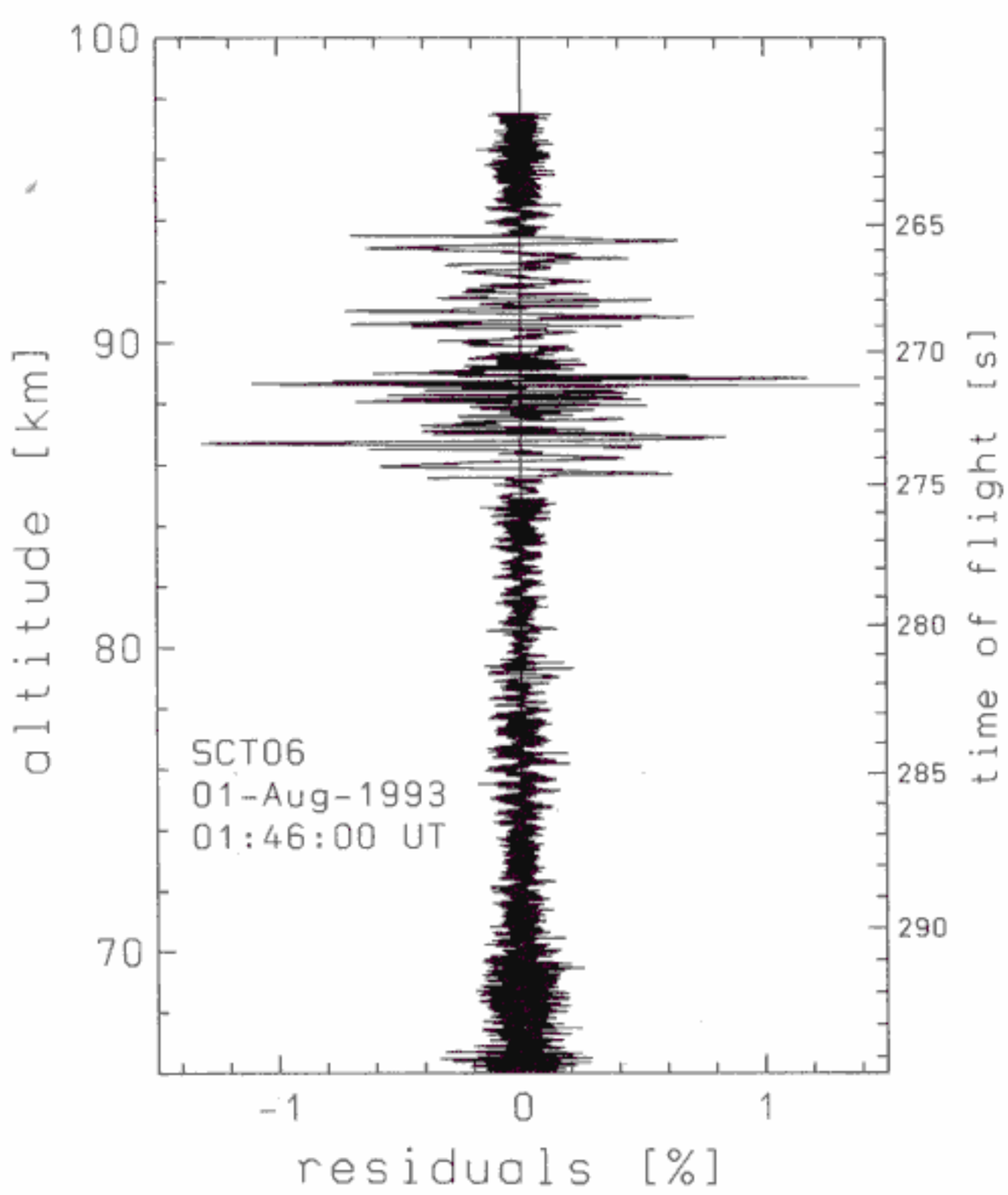

Figure 2. Relative density fluctuations ("residuals") in percent from flight SCT6 performed during the SCALE campaign in summer 1993. Fluctuations exceeding the noise level of ~0.1% are present in the altitude range 85–94 km. The rocket time of flight is shown on the right axis.

Figure 5 shows all ϵ profiles measured during summer except for flight ECT2, which was already shown in Figure 4. Figure 6 shows all profiles measured during the METAL campaign. There are six more winter profiles, which were obtained during the DYANA campaign and were shown by *Hillert et al.* [1994]. There is a systematic difference between the 12 winter profiles and the seven summer profiles; whereas in winter, the turbulent layers are spread over the entire mesosphere, the summer layers are obtained in the upper mesosphere only (typical altitude range is between 85 and 95 km). In addition, the heating rates in summer (typically 10–20 K/d) are significantly larger than those in winter (typically 0.1–1 K/d). The common feature in both the summer and the winter profiles is the fact that turbulence occurs in layers of a few kilometers in thickness.

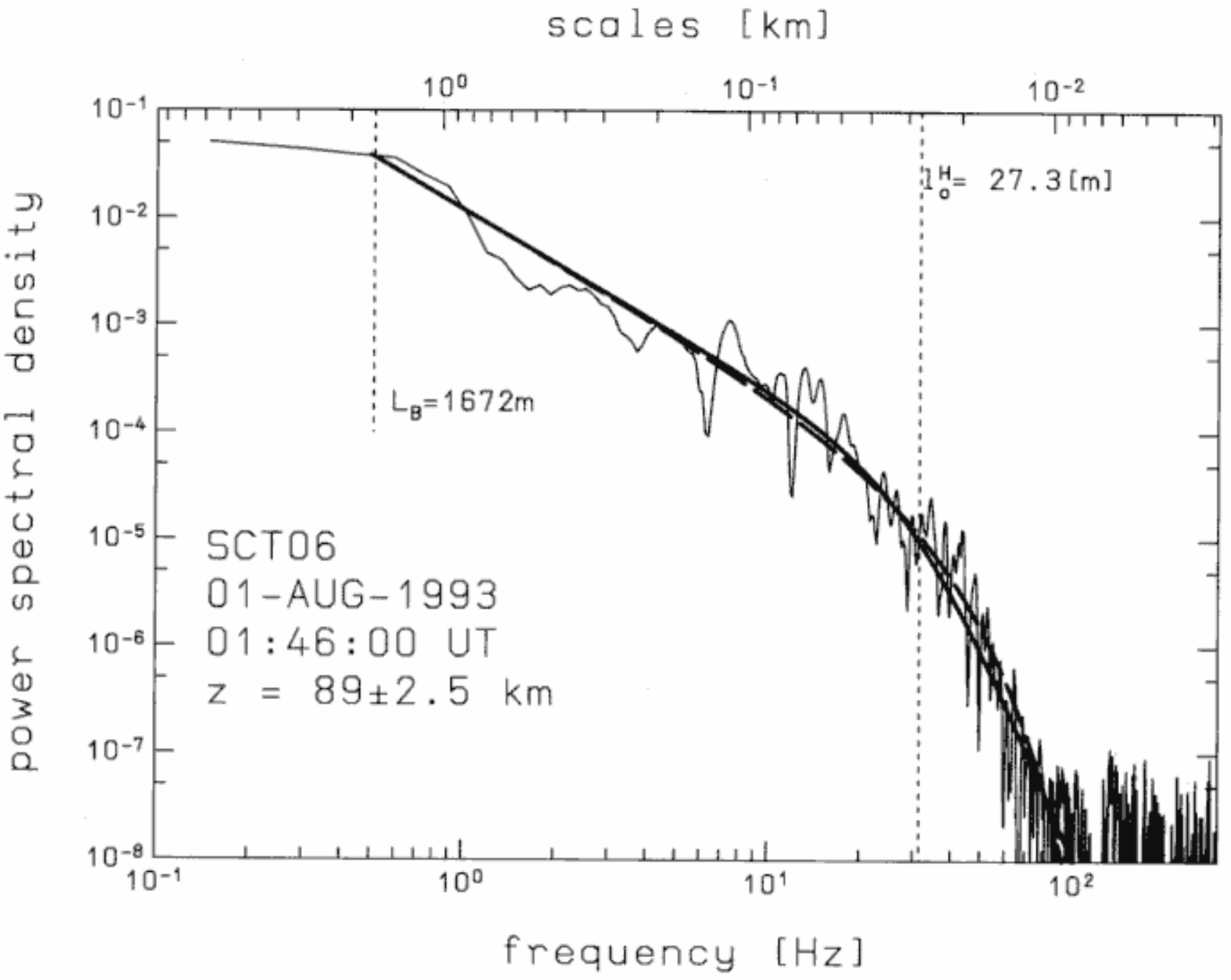

Figure 3. Spectrum of the residuals in the altitude range 89±2.5 km shown in Figure 2. Frequencies f are converted to scales using $\ell = v_R/f$, where v_R=859 m/s is the rocket velocity. The best fit Heisenberg model with an inner scale of ℓ_o^H=27.3 m is shown as a thick dashed line. The Tatarskii model, using the fit parameters from the Heisenberg model, is also shown (thick dotted line).

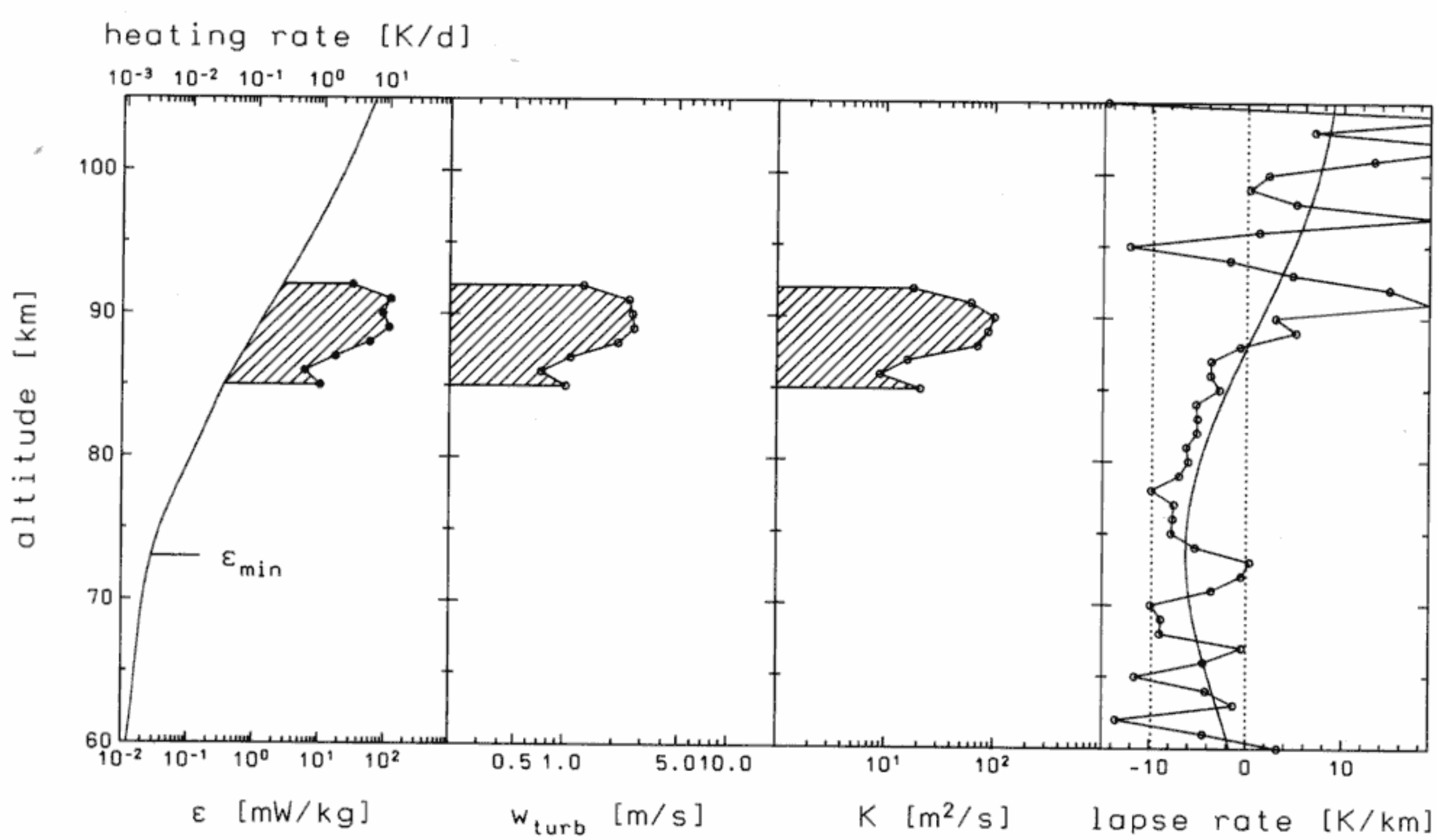

Figure 4. Altitude profiles of the turbulent energy dissipation rate ϵ (heating rates are shown at the top abscissa), the mean turbulent velocity w_{turb}, the turbulent diffusion coefficient K, and the temperature lapse rate for flight ECT2 performed on July 28, 1994, during the ECHO campaign. For comparison we also show the theoretical estimate of the minimum value ϵ_{min} deduced from equation (13) (left panel) and the lapse rate from CIRA 1986 for July and 70°N (smooth solid line in the rightmost panel). The adiabatic lapse rate and the isothermal case are also shown in the rightmost panel (dotted lines).

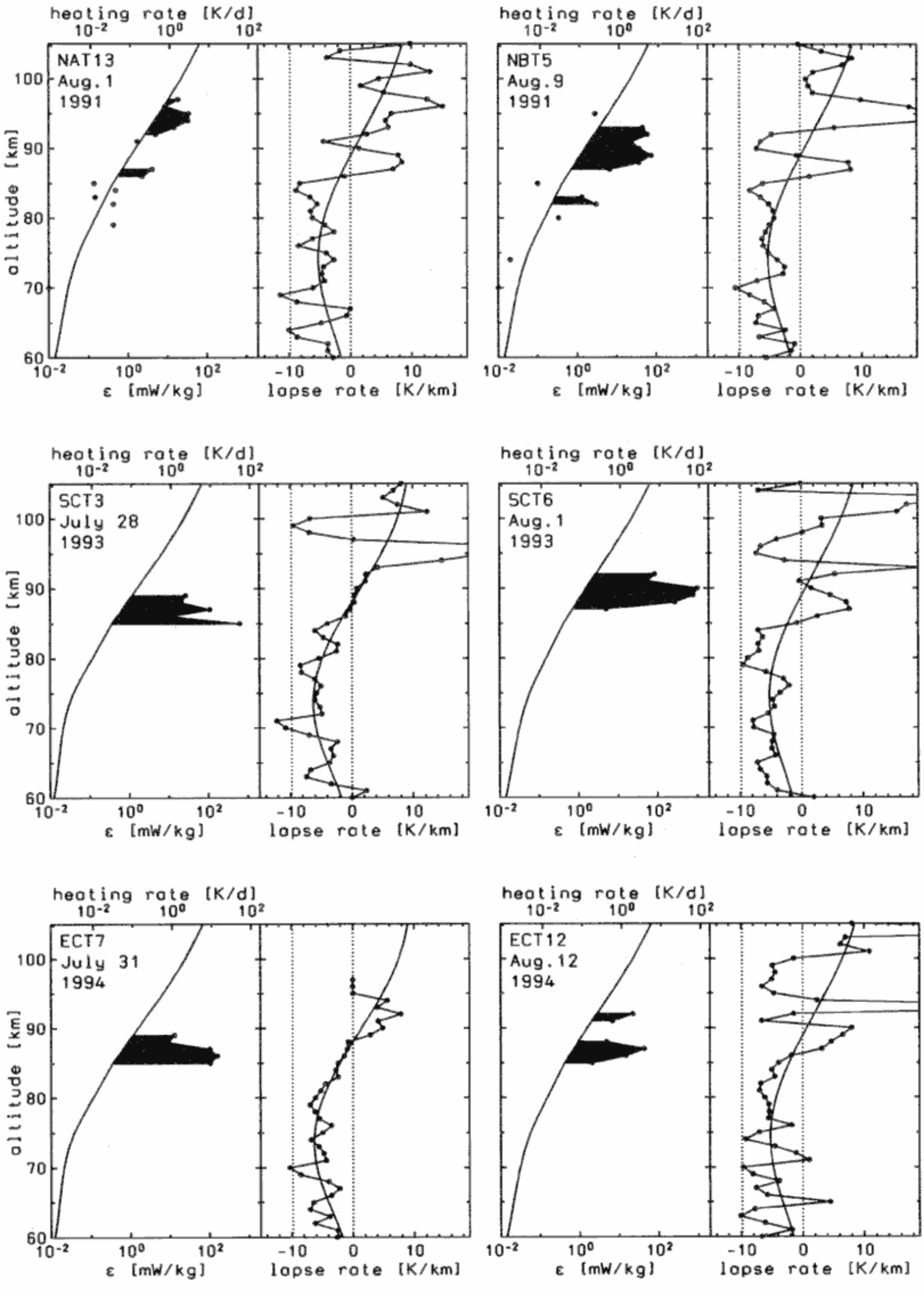

Figure 5. Altitude profiles of the turbulent energy dissipation rate ϵ (heating rates are shown at the top abscissa) and the temperature lapse rate for all summer flights except flight ECT2 shown in Figure 4. We also show the ϵ_{min} profile according to equation (13), the lapse rate from CIRA 1986, and the adiabatic lapse rate and the isothermal case (dotted lines in the rightmost panel). The flight label and the launch time and date are indicated in the plot.

3.3. Mean Profiles

Figure 7 shows all individual ϵ profiles obtained during summer (seven flights). A mean profile is determined by averaging and smoothing the individual measurements with a five-point running mean. The maximum energy dissipation rate is ~150 mW/kg, which is obtained in the altitude region around 90 km. This value corresponds to a heating rate of ~13 K/d, which is of magnitude comparable to that of other contributions to the energy budget in the mesosphere (we will come back to this point in the discussion). No turbulence is observed below ~80 km in any of the seven summer

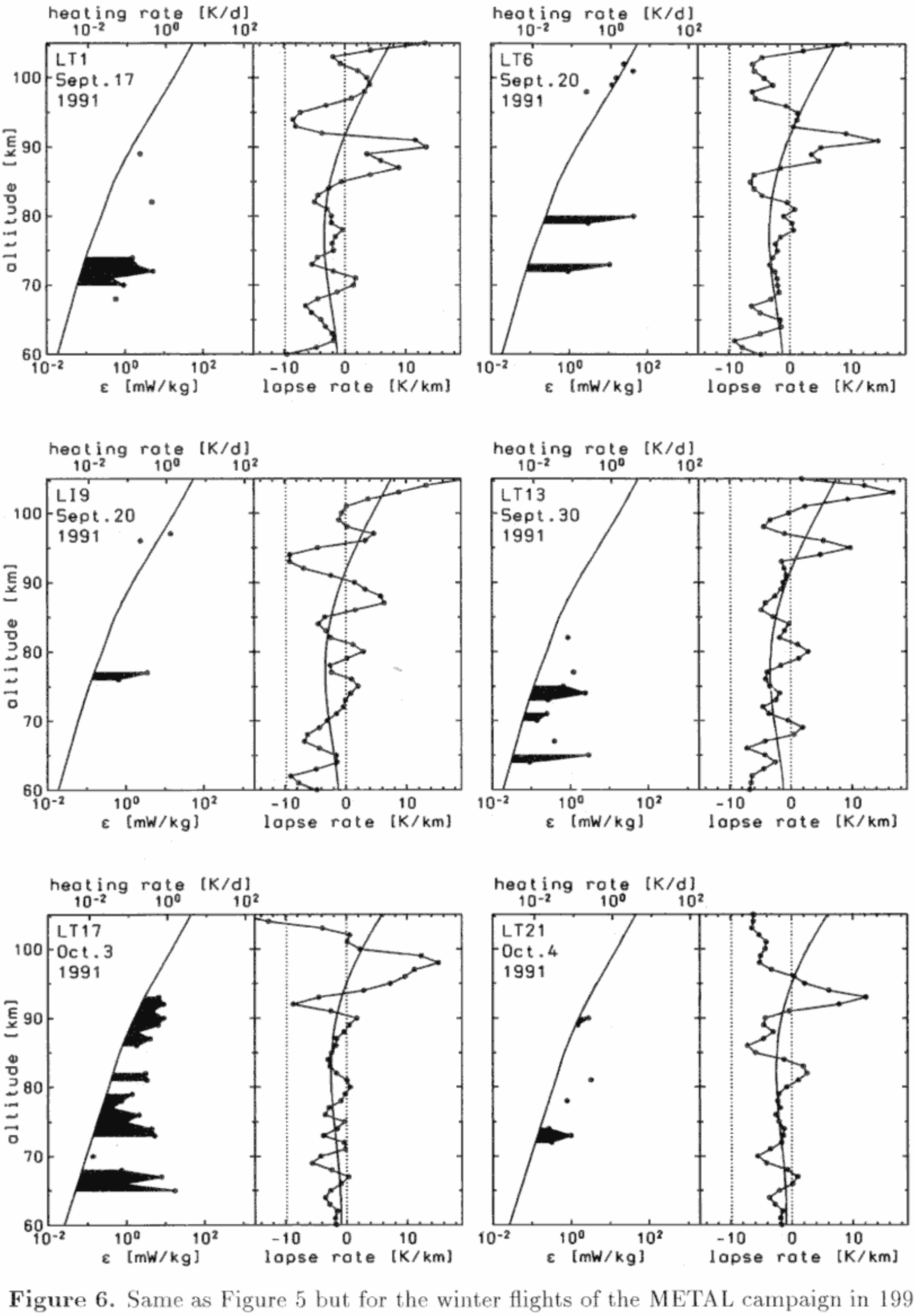

Figure 6. Same as Figure 5 but for the winter flights of the METAL campaign in 1991.

flights. The mean profile has been smoothed further by spline fitting, and the final data are listed in Table 3.

Figure 8 shows all individual ϵ profiles obtained during winter at high latitudes (12 flights). Again, a mean profile for winter is determined by averaging and smoothing the individual measurements. The mean profile of ϵ exhibits a rather smooth altitude dependence in the upper mesosphere with a maximum value of ~20 mW/kg around 90 km. This value corresponds to a heating rate of ~2 K/d, which is almost an order of magnitude smaller than the summer maximum. The energy dissipation rates in the lower mesosphere (below ~77 km) are even smaller with typical values of 1–2 mW/kg (corresponding heating rates of less than 0.2 K/d). The variability of the individual ϵ values at a given altitude is approximately a factor of 5 with no distinct altitude dependence.

The mean profile of Figure 8 has been smoothed further by spline fitting, and the final data are listed in Table 4. These data are very similar to those listed by

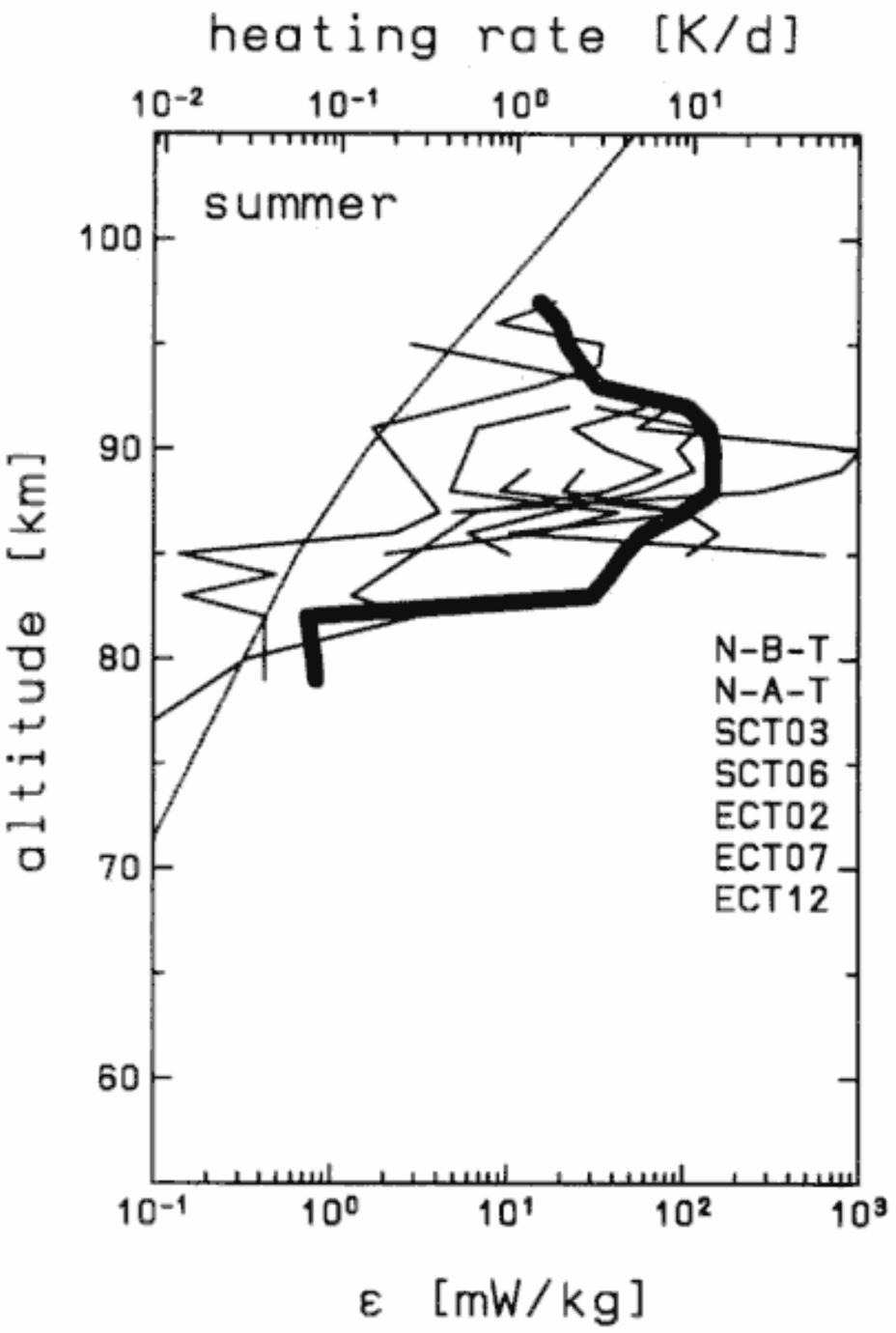

Figure 7. All individual altitude profiles available (seven flights) of the turbulent energy dissipation rate ϵ (heating rates at the top abscissa) obtained with the TOTAL and CONE instrument during summer. The flight labels are indicated in the plot. The mean profile is also shown (thick line). For comparison the theoretical estimate ϵ_{min} deduced from equation (13) is also shown.

Lübken et al. [1993a] (their Table 3), basically because the same flights contribute to both profiles. The main difference is that *Lübken et al.* [1993a] averaged the campaign means, whereas all individual profiles were averaged and smoothed for the data listed here in Table 4. This was done in order to perform a consistent data processing for both the summer and the winter data. The difference between the data listed in Table 4 and those by *Lübken et al.* [1993a] is typically less then 10%, which is negligible for our further discussions.

As can be seen from Figures 7 and 8, turbulence is confined to a relatively small height region of 78–97 km during summer but covers the entire mesosphere from 60 to 100 km during winter. A comparison of the mean summer and winter profile of the smoothed turbulent energy dissipation rates is plotted in Figure 9 together with the theoretical estimate for the lower limit, ϵ_{min}, and the range of global values listed in CIRA (1986). We will come back to a comparison of our data with CIRA (1986) in section 4.

Figures 10 and 11 show the mean smoothed profiles of the turbulent velocity w_{turb} and the turbulent diffusion coefficient K, respectively, for summer and for winter. Typical turbulent velocities in winter are 0.3 and 1-2 m/s below and above ~75 km, respectively. In summer, w_{turb} reaches approximately 3 m/s around 90 km. Turbulent diffusion coefficients are typically 50–150 m^2/s above an altitude of ~80 km. They show only little variation with season, which is within the variability of the individual profiles. We repeat our reservation concerning the absolute values of w_{turb} and K, which are much more uncertain in comparison with ϵ because of the limitations and the stringent assumptions in the derivation of equations (4) and (5).

4. Discussion

4.1. Is There Any Systematical Bias in the Rocket Data?

We will now discuss whether the seasonal variation of our mean turbulent parameters could be systematically biased because of instrumental effects. We have mentioned earlier that the sensitivity of our experimental method is reduced in the summer mesosphere, since the magnitude of the neutral density fluctuations for a given air parcel excursion caused by turbulent motions is proportional to ω_B^2 (see equation (1)), which is smaller in the summer mesosphere than in the winter mesosphere. Does this reduction explain the fact that we do not obtain turbulence below ~85 km in summer? There are several arguments why this is very unlikely. Most

Table 3. Mean Turbulent Parameters for Summer Near 70°N Latitude

z, km	ϵ, mW/kg	dT/dt, K/d	w_{turb}, m/s	K, m^2/s
97.0	15.8	1.36	0.92	16.3
96.0	18.9	1.63	1.03	18.2
95.0	21.7	1.87	1.11	21.2
94.0	26.7	2.30	1.24	29.3
93.0	42.2	3.63	1.52	51.3
92.0	86.1	7.42	2.01	103.
91.0	136.	11.7	2.42	159.
90.0	156.	13.5	2.58	183.
89.0	155.	13.4	2.56	180.
88.0	136.	11.7	2.38	161.
87.0	98.3	8.47	2.01	132.
86.0	67.4	5.81	1.58	108.
85.0	52.7	4.54	1.27	93.1
84.0	37.4	3.22	0.98	67.9
83.0	12.6	1.08	0.65	28.0
82.0	1.90	0.16	0.39	6.72
81.0	0.76	0.07	0.30	2.69
80.0	0.70	0.06	0.28	1.91
79.0	0.81	0.07	0.28	1.71

Here, z is altitude, ϵ is turbulent energy dissipation rate, dT/dt is heating rate, w_{turb} is turbulent velocity, and K is turbulent diffusion coefficient. The profiles contributing to the mean were obtained by the TOTAL instrument during NLC 1991 and by the CONE instrument during SCALE 1993 and ECHO 1994. The flights were performed at high latitudes (Andøya, 69°, or Kiruna, 68°).

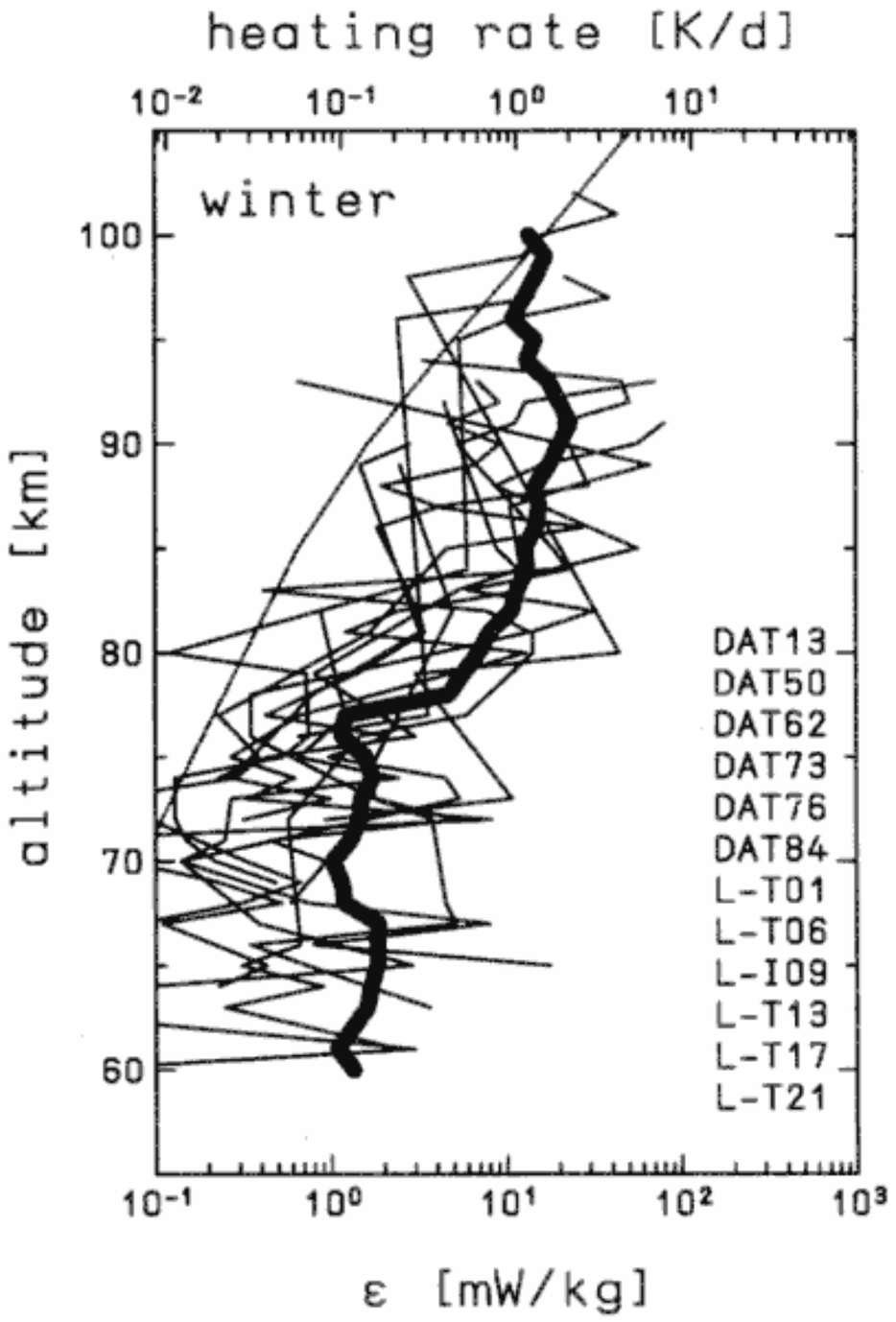

Figure 8. Same as Figure 7 but for winter (total of 12 flights).

important, the sensitivity of our experimental method is still large enough to detect turbulence of significant strength. Using equation (11), we estimate the magnitude of the expected fluctuations for a given energy dissipation rate, a Brunt-Väisälä frequency, and the height interval L_{max} used in our data reduction (1 km in the lower mesosphere). For typical thermal conditions in the summer mesosphere ($dT/dz = -5$ K/km, T=200 K, $\omega_B = 0.015$/s) an energy dissipation rate of 100 mW/kg corresponds to a mean fluctuation (RMS) of 0.7–0.8%. We have never observed this amount of fluctuation in the lower summer mesosphere.

A more simple way to further clarify the arguments above is to assume that the turbulent kinetic energy (or perhaps only a certain fraction of it) is converted to potential energy, which implies vertical excursions of air parcels. For a given kinetic energy with a typical vertical velocity w' (assumed to be completely converted to potential energy) this vertical excursion and the resulting relative density fluctuations are given by

$$\Delta z = w'/\omega_B \quad ; \quad \frac{\Delta n}{n} = \frac{\omega_B}{g} \cdot w' \qquad (14)$$

In the summer mesosphere, where $\omega_B \sim 0.015$/s, a vertical velocity of 4 m/s results in a relative density fluctuation of $\sim$ 0.6%, which requires a vertical excursion of $\sim$ 270 m. We don't observe this magnitude of fluctuations in our 1 km altitude bin.

In summary, we conclude that the reduced sensitivity of our experimental method has no major impact on the mean profile shown in Figure 7. In particular, the fact that we have never observed any significant turbulence in the lower summer mesosphere is most likely a geophysical phenomenon and not an experimental artifact.

Most of our summer flights were performed under polar mesosphere summer echo (PMSE) conditions, which are believed to be somehow related to turbulence (see next section). Could this circumstance have caused a systematic bias of the mean summer profile toward too large values? First, we note that the role of neutral

Table 4. Mean Turbulent Parameters for Winter Near 70°N Latitude

z, km	ϵ, mW/kg	dT/dt, K/d	w_{turb}, m/s	K, m^2/s
100.0	14.6	1.25	1.22	33.1
99.0	15.4	1.32	1.17	29.4
98.0	14.5	1.25	1.11	26.4
97.0	13.0	1.12	1.08	27.7
96.0	12.3	1.06	1.13	40.5
95.0	13.1	1.13	1.23	65.6
94.0	14.6	1.26	1.32	81.4
93.0	17.3	1.49	1.40	97.2
92.0	20.3	1.75	1.45	100.0
91.0	21.8	1.88	1.43	91.5
90.0	20.4	1.76	1.31	66.4
89.0	17.9	1.54	1.16	42.4
88.0	15.9	1.37	1.08	35.0
87.0	15.1	1.30	1.10	43.0
86.0	14.4	1.24	1.17	60.6
85.0	13.5	1.17	1.22	74.8
84.0	12.8	1.10	1.23	79.1
83.0	11.8	1.01	1.17	70.4
82.0	10.3	0.89	1.03	48.4
81.0	8.68	0.75	0.85	27.7
80.0	7.16	0.62	0.70	18.0
79.0	5.41	0.47	0.58	12.3
78.0	3.31	0.28	0.47	7.45
77.0	1.76	0.15	0.38	4.23
76.0	1.33	0.11	0.35	3.40
75.0	1.41	0.12	0.35	3.79
74.0	1.55	0.13	0.35	4.29
73.0	1.54	0.13	0.34	4.27
72.0	1.41	0.12	0.31	3.87
71.0	1.24	0.11	0.29	3.32
70.0	1.11	0.10	0.28	2.89
69.0	1.14	0.10	0.28	2.90
68.0	1.33	0.11	0.30	3.42
67.0	1.64	0.14	0.33	4.39
66.0	1.83	0.16	0.34	5.09
65.0	1.84	0.16	0.34	5.18
64.0	1.72	0.15	0.33	4.85
63.0	1.53	0.13	0.31	4.31
62.0	1.37	0.12	0.29	3.79
61.0	1.22	0.11	0.28	3.28
60.0	1.25	0.11	0.28	3.22

Here, z is altitude, ϵ is turbulent energy dissipation rate, dT/dt is heating rate, w_{turb} is turbulent velocity, and K is turbulent diffusion coefficient. The profiles contributing to the mean were obtained by the TOTAL instrument during the DYANA and the METAL campaign in 1990 and 1991, respectively. Only the flights performed at high latitudes (Andøya, 69°N) were considered.

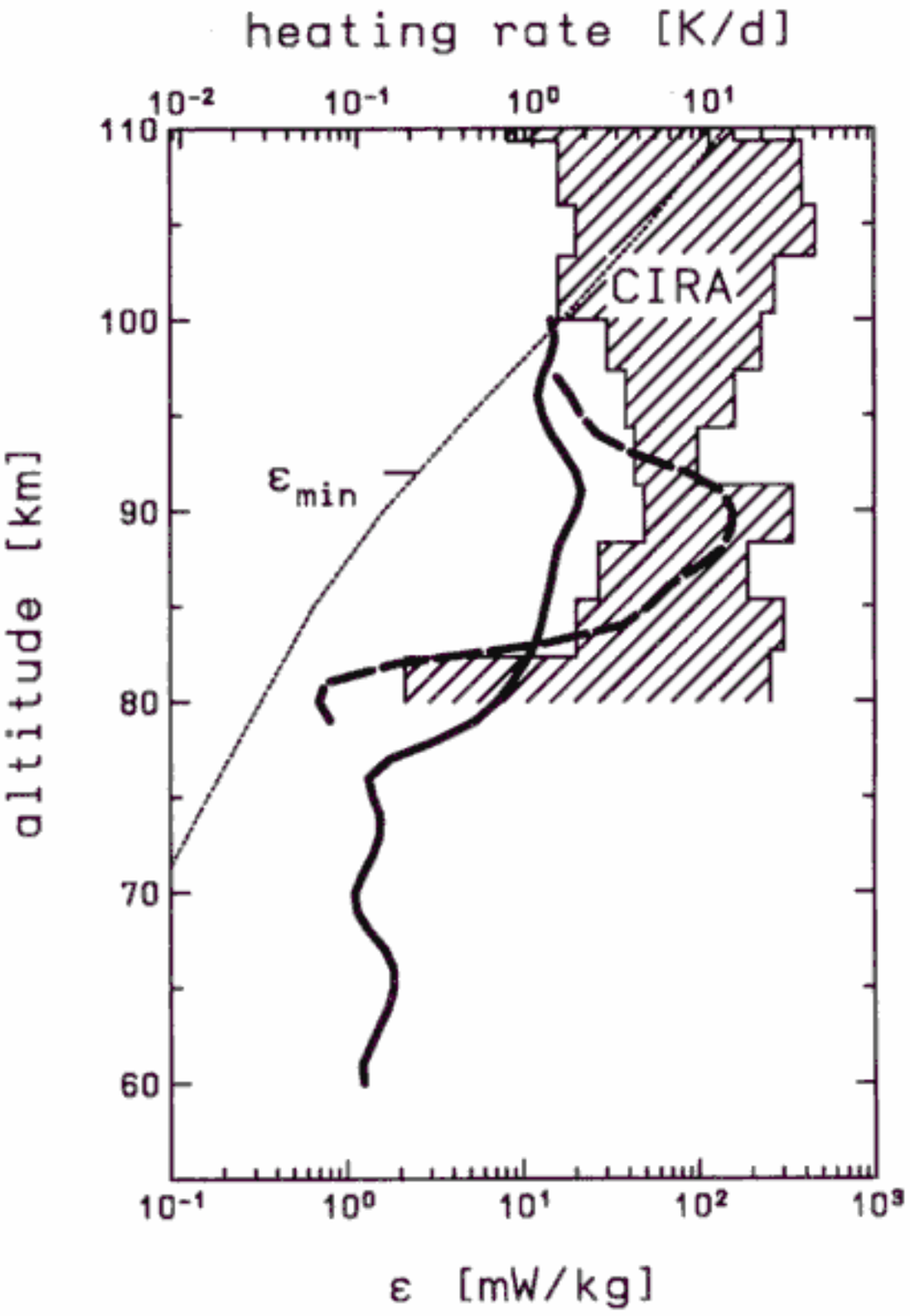

Figure 9. Mean smoothed profiles of the turbulent energy dissipation rate ϵ for summer (dashed line) and winter (solid line) as listed in Tables 3 and 4, respectively. The hatched area shows the range of global ϵ measurements from CIRA 1986 [*Hocking*, 1990]. The ϵ_{min} profile according to equation (13) is also shown (dotted lines).

air turbulence in the creation mechanism of PMSE is not clear at the moment; PMSEs have been observed with and without neutral air turbulence [*Lübken et al.*, 1993b]. Furthermore, PMSE is a very frequent phenomenon in the high-latitude summer mesosphere with an occurrence rate of more than 50% [*Cho and Kelley*, 1993; *Hoffmann et al.*, 1995]. This fact implies that even in the worst case (i.e., if there is no turbulence present at times of no PMSE) the bias in our mean ϵ values in summer would be less than a factor of ~2.

4.2. Comparison With Other Turbulence Measurements

A large number of turbulence measurements using various techniques were compiled for the CIRA (1986) reference atmosphere (see *Hocking* [1990] for more details on the database and the averaging procedure). Figure 9 shows the 67% range of the global energy dissipation rates from CIRA (1986). It is interesting to note that our winter profile is significantly smaller in comparison with CIRA (1986), whereas our summer profile is in rough agreement with this data collection, at least in the upper mesosphere. Please note that most of the measurements contributing to the global CIRA (1986) profile stem from radar techniques, which are somewhat uncertain because of nonturbulent effects on the backscattered signal and/or because of unknown background parameters. In addition, we should keep in mind that most of the radar data in CIRA (1986) were obtained by a MF radar located in Adelaide (35°S), Australia, thus at a very different latitude in comparison with our rocket flights.

Considering high latitudes, *Ecklund and Balsley* [1981] first noted a distinct seasonal modulation of VHF radar echo height and strength in the atmosphere. In particular, very strong echoes, later called "polar mesosphere summer echoes," were observed from around the summer mesopause region [*Ecklund and Balsley*, 1981; *Röttger et al.*, 1988; *Cho and Kelley*, 1993]. The seasonal variation of echo power was commonly taken as an indication of neutral air turbulence, which causes small-scale plasma density fluctuations and therefore creates refractive index variations at the Bragg scale of the radar waves. However, simultaneous in situ observations of neutral and plasma density fluctuations in the presence of PMSE have shown that neutral air turbulence is not necessarily the cause of either the plasma fluctuations or the PMSEs [*Lübken et al.*, 1993b]. On the other hand, there have indeed been a few cases in which neutral air turbulence and strong plasma fluctuations were observed in the vicinity of PMSE, but there is still no simple relationship between PMSE and neutral versus plasma density fluctuations, since the latter extend to smaller scales in comparison with the neutrals. These observations have been interpreted as being due to a reduced molecular diffusion coefficient de-

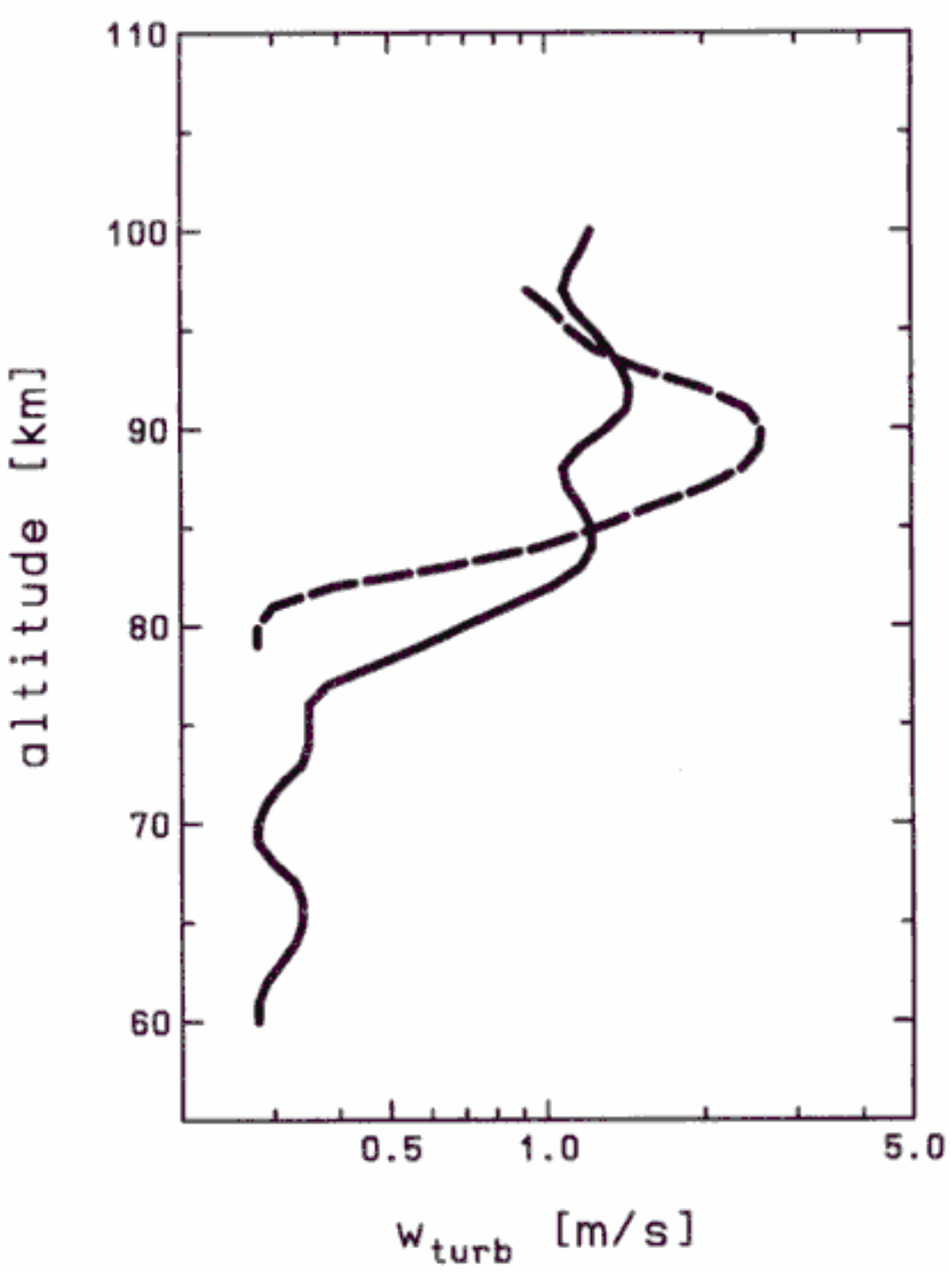

Figure 10. Mean profiles of the mean turbulent velocity for summer (dashed line) and winter (solid line) as listed in Tables 3 and 4, respectively.

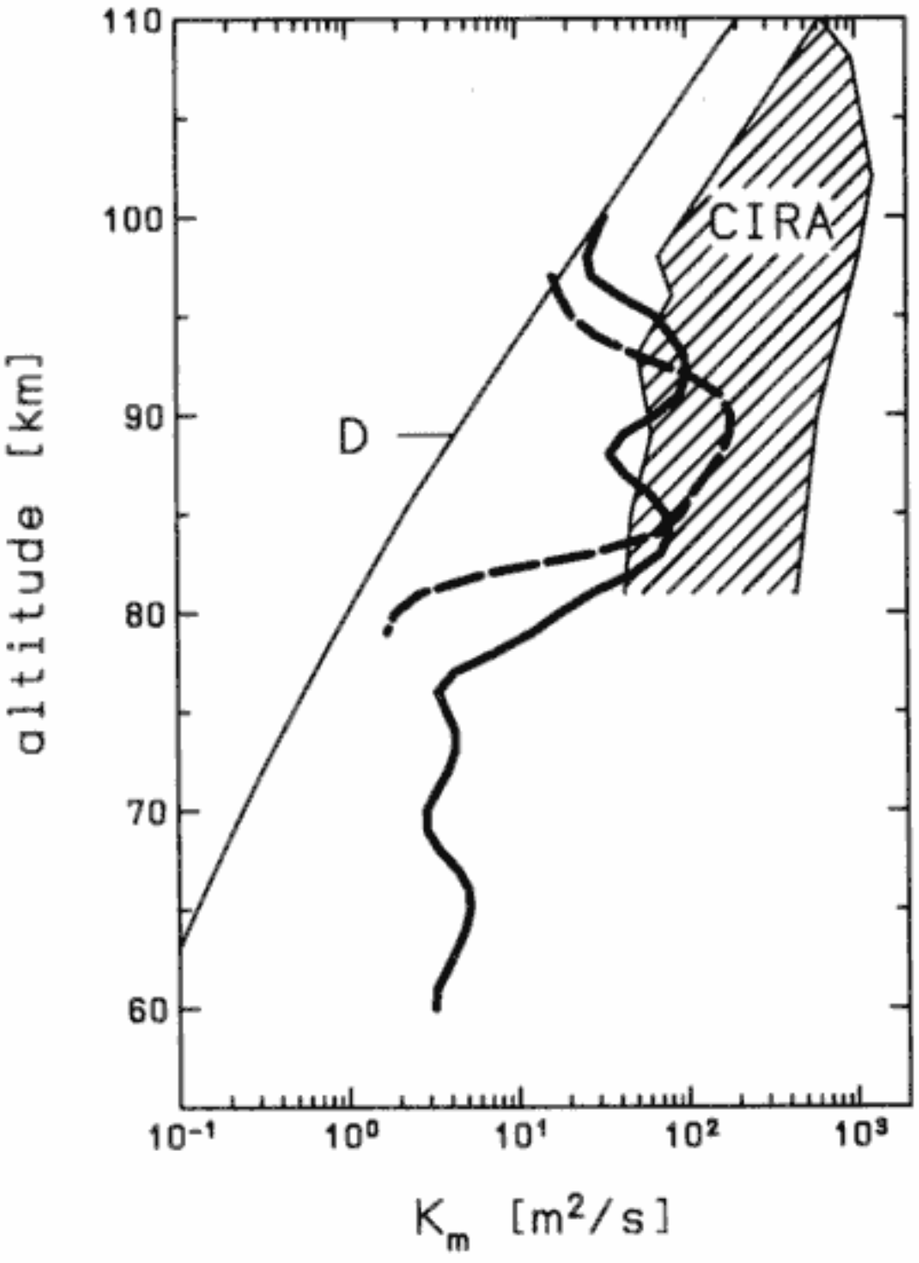

Figure 11. Mean profiles of the turbulent diffusion coefficient K for summer (dashed line) and winter (solid line) as listed in Tables 3 and 4, respectively. The hatched area shows the range of global ϵ measurements from CIRA 1986 [*Hocking*, 1990].

scribed by a Schmidt number larger than unity (the Schmidt number is defined as the ratio of the kinematic viscosity to the molecular diffusion coefficient for the tracer under consideration) [*Kelley et al.*, 1987; *Lübken et al.*, 1994b]. Several theories for the explanation of PMSEs exist; some still involve neutral air turbulence, at least as an indirect or supportive process for creating or maintaining small-scale plasma fluctuations [*Cho and Röttger*, 1997]. We conclude that the role of neutral air turbulence in the creation mechanism for PMSE is still not clear. This conclusion also implies doubts in the interpretation of the seasonal variation of radar echoes. Despite these uncertainties we note that our in situ measurements of turbulence confirm the oversimplified interpretation of the radar echo seasonal variation, showing strong turbulence around the summer mesopause and relatively weak turbulence in the entire mesosphere in winter.

Do radars at lower latitude observe a significant variation of turbulence throughout the season? MF radar measurements performed at Adelaide show a rather smooth semiannual variation of energy dissipation rates with maximum values of $\sim$ 140 mW/kg at solstice and minimum values of $\sim$ 100 mW/kg around the equinoxes [*Hocking*, 1988; *Vandepeer and Hocking*, 1993]. The altitude of these measurements is $\sim$86 km. In a recent paper *Hocking* [1996] has discussed in more detail the procedure to deduce turbulent energy dissipation rates from radar spectral widths. He concludes that modifications need to be made that "...reduce previous radar estimates of energy dissipation rates by up to a factor of 2 or 3." It is not known at the moment whether these modifications also affect the amplitude of the seasonal modulation.

Fukao et al. [1994] have summarized nearly 3 years of VHF radar measurements from Japan (35°N), including turbulent diffusivities K deduced from the radar spectral widths. At mesospheric heights (60–82 km) they found a seasonal maximum of K in summer and only a small semiannual component. It is interesting to note that the difference between summer and winter reaches an order of magnitude, similar to our in situ observations for ϵ at high latitudes (see Figure 9). On the other hand, because of the ω_B dependence of K in equation (5) the difference between our summer and winter mean is smaller in K than it is in ϵ (see Figure 11).

4.3. Comparison With Model Predictions of Turbulence

A detailed comparison of our winter mean profile with models has been performed by *Lübken et al.* [1993a]. Only a few of these models make a prediction on the seasonal variation of turbulent parameters and present energy dissipation rate profiles. Here we will concentrate on a recently published model by *Fritts and Luo* [1995], which specifically concentrates on the high-

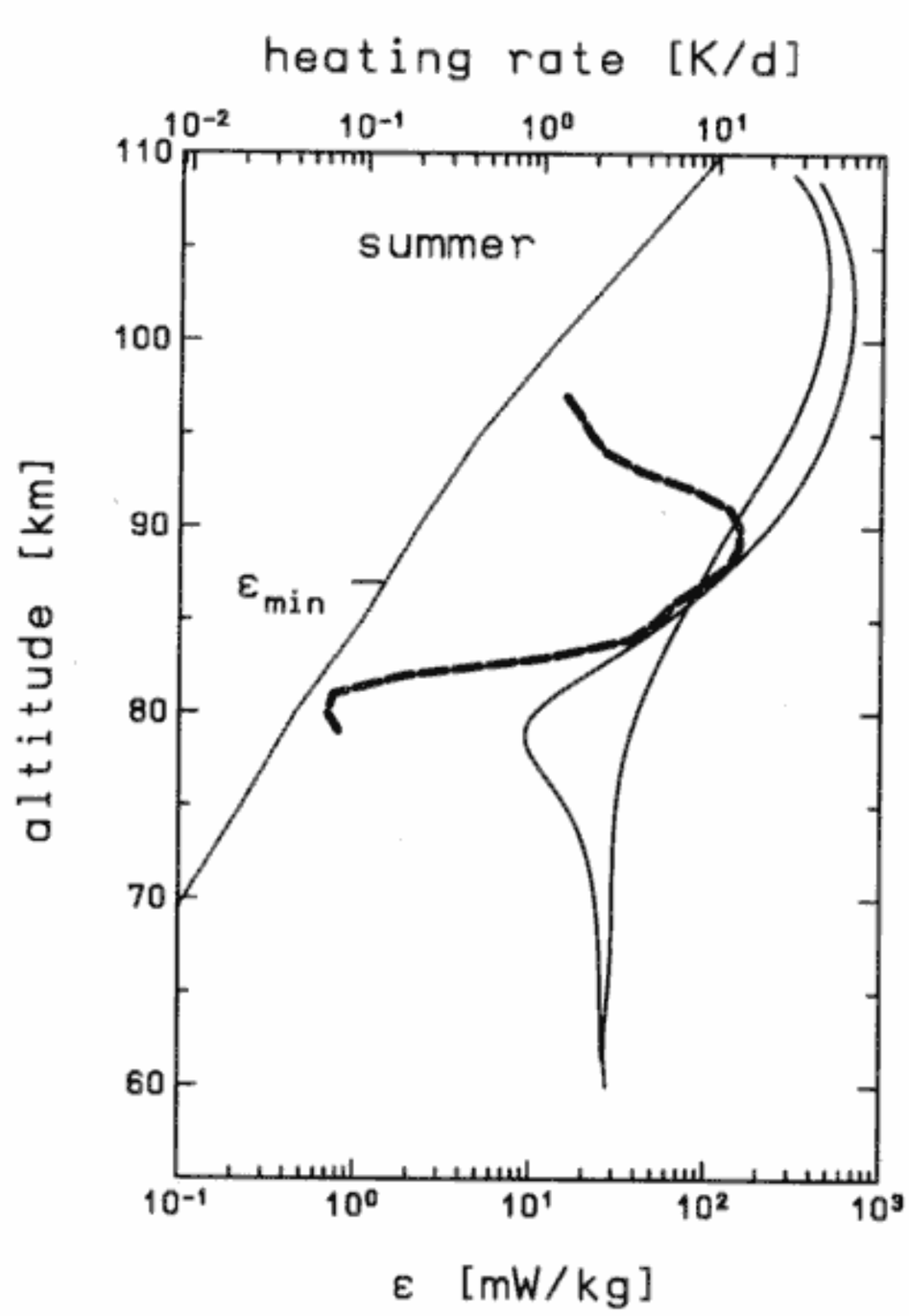

Figure 12. Comparison of our mean energy dissipation rates during summer (thick dashed line) with the model of *Fritts and Luo* [1995] (thin lines). The two lines represent the ϵ variation for various model parameters. The ϵ_{min} profile according to equation (13) is also shown.

latitude mesopause region in summer. In Figure 12 the results from this model are plotted together with our mean summer profile. As a common feature in the data and in the model the energy dissipation rates are comparatively small in the lower mesosphere and increase significantly around 80–85 km. The largest difference between the model and the measurements is observed in the lower mesosphere and in the lower thermosphere, where the model predicts significantly larger ϵ values in comparison with our measurements. To express this difference in terms of density fluctuations, we have determined the magnitude of the expected fluctuations for the model energy dissipation rates from equation (11), using the appropriate Brunt-Väisälä frequencies, and the height interval L_{max} of our data reduction (1 and 5 km in the lower mesosphere and in the lower thermosphere, respectively). For model energy dissipation rates of 20 and 700 mW/kg at 65 km and 100 km, respectively, we arrive at relative density fluctuations (RMS) of 0.4% and 4.5%, respectively. We do not observe these kinds of large fluctuations in the lower mesosphere and thermosphere, respectively (we should not forget, however, the uncertainties in the parameters used in equation (11)). We conclude that the difference between our mean ϵ profile in summer and the model of *Fritts and Luo* [1995] cannot be explained by experimental constraints but should be accounted for by modifying the model parameters. We note that the ϵ values calculated from this model may be considered an upper limit, because gravity waves may lose energy by processes other than turbulence. In addition, the Fritts and Luo model was tuned to the mesopause region and thus is rather speculative at greater and lower altitudes.

Garcia and Solomon [1985, their Figure 10] have determined the seasonal variation of the eddy diffusion coefficients for 61°N from their two-dimensional dynamical/chemical model. We have noted earlier the difficulties in comparing turbulent diffusion coefficients from measurements and from models, since the physical processes involved may be very different and it may not be clear how they are interrelated. Despite these difficulties we note that there are considerable similarities between the *Garcia and Solomon* [1985] model and our experimental results; the maximum turbulent activity is located in the summer season around 90 km, with a steep drop-off below ~80 km. Both this model and our data show a much smoother height dependence in winter than in summer.

In a recent model simulation, *Alexander* [1996] has studied the propagation and breaking of convectively generated gravity waves for mean conditions during April and June. In June the filtering effect of the mean winds at lower altitudes causes the gravity waves to dissipate their energy in a fairly limited layer between 72 and 90 km (peak at 82 km). During April, however, the altitude range of wave breaking is larger and extends into the lower mesosphere. In addition, the peak ϵ values are considerably larger in June than in April. These results are in good agreement with our observations (see Figure 9), suggesting that convectively generated gravity waves may contribute significantly to the total wave source in the troposphere.

4.4. Comparison of Energy Dissipation Rates With Other Atmospheric Quantities

The importance of heating due to turbulent energy dissipation can only be judged adequately if the other contributions to the energy budget of the upper atmosphere are known, at least to a reasonably good approximation. Unfortunately, we are far from a complete understanding of the thermal budget of the upper atmosphere, and the contributions from the various processes involved are rather uncertain. We note, however, that our maximum turbulent heating rate of 10–20 K/d in summer is comparable to, or even larger than, the other heating or cooling mechanisms believed to be important in the mesopause region. Apart from turbulence the main contributions are from adiabatic cooling due to strong upwelling, radiative and chemical heating, radiative cooling, and the thermal effects of gravity wave breaking (heating and cooling, e.g., by heat transport) [*Walterscheid*, 1981; *Garcia and Solomon*, 1985; *Dickinson et al.*, 1987; *Huang and Smith*, 1991; *Mlynczak and Solomon*, 1993; *Riese et al.*, 1994; *Fomichev et al.*, 1996]. We conclude that turbulent heating plays a major role in the energy budget of the upper mesosphere, at least at mesopause altitudes during summer.

It is interesting to compare the seasonal variation of ϵ with the thermal structure of the mesosphere, which is very different in winter from that in summer. Whereas in winter the temperature profiles show large variability in the mesosphere, the thermal structure is very stable in summer. The mesopause is located around 100 km in winter and at ~88 km during summer [*Lübken and von Zahn*, 1991]. We note that at high latitudes in summer the mesopause height is very close to the altitude at which our mean ϵ profile exhibits a maximum (see Figure 9). This finding implies that maximum turbulent activity is observed in a region of increased static stability, which is in excellent agreement with the expectation from gravity wave breaking theory applied to summer polar mesopause conditions [e.g., *McIntyre*,1989].

5. Conclusions

In summary, a total of 22 TURBO sounding rocket flights were performed in the years 1990–1995, all of which were successful and gave scientific data. With our ionization gauges on board the TURBO payloads we have measured relative neutral gas densities in the mesosphere and lower thermosphere with an unprecedented spatial resolution of a few meters. This high resolution allows one to apply a recently developed theoretical method to unambiguously deduce turbulent en-

ergy dissipation rates from the spectra of the density fluctuation. At high latitudes, seven flights were performed during summer, and 12 flights were performed during winter and autumn. Taking into account the seasonal variation of the thermal structure in the high latitude mesosphere, the autumn flights were grouped into the "winter" category.

Neutral density fluctuations indicative of turbulence were found in layers of a few kilometers in thickness, both in summer and in winter. The height coverage of these layers exhibits a significant and systematic variation with season: Turbulence is confined to a relatively small height region of 78–97 km during summer but covers the entire mesosphere from 60 to 100 km during winter.

The mean turbulent energy dissipation rate profiles also exhibit a significant seasonal dependence. In summer the maximum ϵ values of ~150 mW/kg are found around 90 km. The corresponding heating rate of ~13 K/d is comparable in magnitude with other heat sources present in the upper mesosphere. In winter, typical mean energy dissipation rates are 10–20 mW/kg (heating rates of 1–2 K/d) at 80–100 km, considerably smaller than summer rates. Even smaller ϵ values are observed below 75 km in winter. In general, the turbulent heating rates in winter are presumably negligible in comparison with other heat sources present in the mesosphere.

Our observations lead to the curious conclusion that the strongest turbulent heating in the mesosphere and lower thermosphere occurs at the coldest place in the entire terrestrial atmosphere, namely, at the polar mesopause in summer. This heating has to be compensated for by cooling mechanisms, such as radiative cooling, turbulent heat conduction, and adiabatic cooling due to mean upward motions.

The seasonal variation of turbulent activity observed in the mesosphere is presumably caused by breaking gravity waves, which are generated in the troposphere and filtered by the seasonal dependent prevailing winds in the middle atmosphere. Our experimental results put a serious constraint on models dealing with the energy budget of the upper atmosphere, in particular their dependence on gravity wave induced sources and sinks of heat. The parameterization of subgrid processes in terms of mean quantities used in these models must be compatible with our mean ϵ profiles and their seasonal variation.

Acknowledgments. I am grateful to my colleagues Hinnerk Baumann, Simone Berendonck, Frank Föhner, Jochen Giebeler, Wolfgang Hillert, Gerald Lehmacher, and Martin Nägele for their support in preparing, conducting, and evaluating the TOTAL and CONE flights. I thank my colleague Karl-Heinz Fricke for helpful discussions and comments. The support from Ulf von Zahn throughout the TURBO project is appreciated. The excellent work by the crew of the Mobile Raketenbasis (Germany), the Andøya Rocket Range (Norway), and the Esrange Facility (Sweden) is gratefully acknowledged. The rocket flights were supported by the Bundesministerium für Bildung, Wissenschaft, Forschung und Technologie under DARA grant 01OE88027.

References

Alexander, M. J., A simulated spectrum of convectively generated gravity waves: Propagation from the tropopause to the mesopause and effects in the middle atmosphere, *J. Geophys. Res.*, *101*, 1571–1588, 1996.

Alpers, M., T. Blix, S. Kirkwood, D. Krankowsky, F.-J. Lübken, S. Lutz, and U. von Zahn, First simultaneous measurements of neutral and ionized iron densities in the upper mesosphere, *J. Geophys. Res.*, *98*, 275–283, 1993.

Blamont, J.-E., and C. DeJager, Upper atmospheric turbulence near the 100 km level, *Ann. Geophys.*, *17*, 134–144, 1961.

Blix, T. A., E. V. Thrane, and O. Andreassen, In situ measurements of fine-scale structure and turbulence in the mesosphere and lower thermosphere by means of electrostatic positive ion probes, *J. Geophys. Res.*, *95*, 5533–5548, 1990.

Cho, J. Y. N., and M. C. Kelley, Polar mesosphere summer radar echoes: Observations and current theories, *Rev. Geophys.*, *31*, 243–265, 1993.

Cho, J. Y. N., and J. Röttger, An updated review of polar mesosphere summer echoes: Observation, theory, and their relationship to noctilucent clouds and subvisible aerosols, *J. Geophys. Res.*, *102*, 2001–2020, 1997.

Dickinson, R. E., R. G. Roble, and S. W. Bougher, Radiative cooling in the NLTE region of mesosphere and lower thermosphere – global energy balance, *Adv. Space Res.*, 7(10), 5–15, 1987.

Ecklund, W. L., and B. B. Balsley, Long-term observations of the arctic mesosphere with the MST radar at Poker Flat, Alaska, *J. Geophys. Res.*, *86*, 7775–7780, 1981.

Fomichev, V. I., W. E. Ward, and C. McLandress, Implications of variations in the 15 μm CO_2 band cooling in the mesosphere and lower thermosphere associated with current climatologies of the atomic oxygen mixing ratio, *J. Geophys. Res.*, *101*, 4041–4055, 1996.

Fritts, D. C., and Z. Luo, Dynamical and radiative forcing of the summer mesopause circulation and thermal structure, 1, Mean solstice conditions, *J. Geophys. Res.*, *100*, 3119–3128, 1995.

Fukao, S., M. D. Yamanaka, N. Ao, W. K. Hocking, T. Sato, M. Yamamoto, T. Nakamura, T. Tsuda, and S. Kato, Seasonal variability of vertical eddy diffusivity in the middle atmosphere, 1, Three-year observations by the middle and upper atmosphere radar, *J. Geophys. Res.*, *99*, 18,973–18,987, 1994.

Gage, K. S., and B. B. Balsley, MST radar studies of wind and turbulence in the middle atmosphere, *J. Atmos. Terr. Phys.*, *46*, 739–753, 1984.

Garcia, R. R., and S. Solomon, The effect of breaking gravity waves on the dynamics and chemical composition of the mesosphere and lower thermosphere, *J. Geophys. Res.*, *90*, 3850–3868, 1985.

Goldberg, R., E. Kopp, G. Witt, and W. Swartz, An overview of NLC-91: A rocket/radar study of the polar summer mesosphere, *Geophys. Res. Lett.*, *20*, 2443–2446, 1993.

Hillert, W., F.-J. Lübken, and G. Lehmacher, TOTAL: A rocket-borne instrument for high resolution measurements of neutral air turbulence during DYANA, *J. Atmos. Terr. Phys.*, *56*, 1835–1852, 1994.

Hocking, W., Turbulence in the region 80-120 km, *Adv. Space Res.*, *10*(12), 153–161, 1990.

Hocking, W., An assessment of the capabilities and limi-

tations of radars in measurements of upper atmosphere turbulence, *Adv. Space Res.*, *17*(11), 37–47, 1996.
Hocking, W. K., Measurement of turbulent energy dissipation rates in the middle atmosphere by radar techniques: A review, *Radio Sci.*, *20*, 1403–1422, 1985.
Hocking, W. K., Two years of continuous measurements of turbulence parameters in the upper mesosphere and lower thermosphere made with a 2-MHz radar, *J. Geophys. Res.*, *93*, 2475–2492, 1988.
Hoffmann, P., J. Bremer, W. Singer, R. Rüster, and A. Manson, PMSE observations with the ALOMAR-SOUSY radar and the EISCAT VHF radar during summer 1994, in *Proceedings of the 12th ESA Symposium on European Rocket and Balloon Programmes and Related Research, Lillehammer, Norway, ESA Spec. Publ., SP–370*, pp. 73–80, Eur. Space Agency, Neuilly, France, 1995.
Huang, T. Y. W., and A. K. Smith, The mesospheric diabatic circulation and the parameterized thermal effect of gravity wave breaking on the circulation, *J. Atmos. Sci.*, *48*, 1093–1111, 1991.
Jones, J., and J. W. Peterson, Falling sphere measurements, 30 to 120 km, *Meteorol. Monogr.*, *8*, 176–177, 1968.
Kelley, M. C., D. T. Farley, and J. Röttger, The effect of cluster ions on anomalous VHF backscatter from the summer polar mesosphere, *Geophys. Res. Lett.*, *14*, 1031–1034, 1987.
Lehmacher, G., and F.-J. Lübken, Simultaneous observation of convective adjustment and localized turbulence production in the mesosphere, *Geophys. Res. Lett.*, *22*, 2477–2480, 1995.
Lübken, F.-J., On the extraction of turbulent parameters from atmospheric density fluctuations, *J. Geophys. Res.*, *97*, 20,385–20,395, 1992.
Lübken, F.-J., Rocket-borne measurements of small scale structures and turbulence in the upper atmosphere, *Adv. Space Res.*, *17*(11), 25–35, 1996.
Lübken, F.-J., Aerodynamical effects in number density measurements in the lower thermosphere with the CONE instrument, *Adv. Space Res.*, *19*(1), 139–144, 1997.
Lübken, F.-J., and T. Blix, The SCALE 1993 campaign, *STEP Bull.*, *4*(4), 1–2, 1994.
Lübken, F.-J., and U. von Zahn, Thermal structure of the mesopause region at polar latitudes, *J. Geophys. Res.*, *96*, 20,841–20,857, 1991.
Lübken, F.-J., W. Hillert, G. Lehmacher, and U. von Zahn, Experiments revealing small impact of turbulence on the energy budget of the mesosphere and lower thermosphere, *J. Geophys. Res.*, *98*, 20,369–20,384, 1993a.
Lübken, F.-J., G. Lehmacher, T. Blix, U.-P. Hoppe, E. Thrane, J. Cho, and W. Swartz, First in-situ observations of neutral and plasma density fluctuations within a PMSE layer, *Geophys. Res. Lett.*, *20*, 2311–2314, 1993b.
Lübken, F.-J., W. Hillert, G. Lehmacher, U. von Zahn, M. Bittner, D. Offermann, F. Schmidlin, A. Hauchecorne, M. Mourier, and P. Czechowsky, Intercomparison of density and temperature profiles obtained by lidar, ionization gauges, falling spheres, datasondes, and radiosondes during the DYANA campaign, *J. Atmos. Terr. Phys.*, *56*, 1969–1984, 1994a.
Lübken, F.-J., J. Giebeler, T. Blix, E. Thrane, W. Singer, and J. Bremer, In-situ measurement of the Schmidt number within a PMSE layer, *Geophys. Res. Lett.*, *21*, 1651–1654, 1994b.
Lübken, F.-J., W. Hillert, G. Lehmacher, U. von Zahn, T. Blix, E. Thrane, H.-U. Widdel, G. A. Kokin, and A. K. Knyazev, Morphology and sources of turbulence in the mesosphere during DYANA, *J. Atmos. Terr. Phys.*, *56*, 1809–1833, 1994c.
Lübken, F.-J., K.-H. Fricke, and M. Langer, Noctilucent clouds and the thermal structure near the arctic mesopause, *J. Geophys. Res.*, *101*, 9489–9508, 1996.
McIntyre, M. E., On dynamics and transport near the polar mesopause in summer, *J. Geophys. Res.*, *94*, 14,617–14,628, 1989.
Mlynczak, M. G., and S. Solomon, A detailed evaluation of the heating efficiency in the middle atmosphere, *J. Geophys. Res.*, *98*, 10,517–10,541, 1993.
Offermann, D., The DYANA campaign: A survey, *J. Atmos. Terr. Phys.*, *56*, 1639–1658, 1994.
Rees, D., R. G. Roper, K. H. Lloyd, and C. H. Low, Determination of the structure of the atmosphere between 90 and 250 km by means of contaminant releases at Woomera, May 1968, *Philos. Trans. R. Soc. London*, *271*, 631–663, 1972.
Riese, M., D. Offermann, and G. Brasseur, Energy released by recombination of atomic oxygen and related species at mesopause heights, *J. Geophys. Res.*, *99*, 14,585–14,593, 1994.
Röttger, J., C. LaHoz, M. C. Kelley, U.-P. Hoppe, and C. Hall, The structure and dynamics of polar mesosphere summer echoes observed with the EISCAT 224 MHz radar, *Geophys. Res. Lett.*, *15*, 1353–1356, 1988.
Schmidlin, F. J., The inflatable sphere: A technique for the accurate measurement of middle atmosphere temperatures, *J. Geophys. Res.*, *96*, 22,673–22,682, 1991.
Tatarskii, V. I., *The Effects of the Turbulent Atmosphere on Wave Propagation*, Isr. Program for Sci. Transl., Jerusalem, 1971.
Thrane, E. V., and B. Grandal, Observations of fine scale structure in the mesosphere and lower thermosphere, *J. Atmos. Terr. Phys.*, *43*, 179–189, 1981.
Vandepeer, B. G., and W. Hocking, A comparison of Doppler and spaced antenna radar techniques for the measurement of turbulent energy dissipation rates, *Geophys. Res. Lett.*, *20*, 17–20, 1993.
Walterscheid, R. L., Dynamical cooling induced by dissipating internal gravity waves, *Geophys. Res. Lett.*, *8*, 1235–1238, 1981.
Weinstock, J., Vertical turbulent diffusion in a stably stratified fluid, *J. Atmos. Sci.*, *35*, 1022–1027, 1978.
Weinstock, J., Energy dissipation rates of turbulence in the stable free atmosphere, *J. Atmos. Sci.*, *38*, 880–883, 1981.
Wu, Y.-F., and H.-U. Widdel, Turbulent energy dissipation rates and eddy diffusion coefficients derived from foil cloud measurements, *J. Atmos. Terr. Phys.*, *51*, 497–506, 1989.

F.-J. Lübken, Physikalisches Institut der Universität Bonn, Nussallee 12, 53115 Bonn, Germany. (e-mail: luebken@physik.uni-bonn.de)

(Received May 16, 1996; revised February 24, 1997; accepted March 17, 1997.)